PAPER

🔴 Check for updates

Nature-inspired preparation of self-adhesive, frost-resistant, and ion-conductive hydrogels for flexible strain sensors†

Tiantian Zhang,[a] Lihui Meng,[a] Yanru Hu,[a] Zhiyuan Ouyang,[a] Wenchao Li,[a] Bin Xie,[a] Fang Zhu,[a] Jiangling Wan*[b] and Qingzhi Wu 🆔 *[a]

A nature-inspired strategy has been developed to prepare polyvinyl alcohol (PVA)/catechol-modified quaternized chitosan (QCS-C)/MXene hydrogels with good self-adhesion, frost-resistance, and high ion-conductivity. The PVA/QCS-C/MXene hydrogel shows an ionic conductivity of 8.82 S m^{-1} and a gauge factor of 33.53 at low strain (0–10%), and remains flexible and conductive at −47 °C. The PVA/QCS-C$_{15}$/MXene hydrogel displays promising potential as an ionically conductive hydrogel sensor for applications in flexible electronic devices.

1. Introduction

Flexible sensors with high performance[1,2] have attracted increasing interest due to the characteristics of high flexibility, sensitivity, and fast response in the fields of artificial intelligence, smart healthcare, and the Internet of Things.[3,4] Traditional flexible sensors are usually composed of a stretchable matrix and conductive components, and include conductive polymers,[5,6] carbon nanomaterials,[7,8] metal and metal oxide nanoparticles,[9,10] and semiconductors.[11,12] Flexible sensors are ready to withstand different deformations (such as tensile, bending, and compressive deformation) and convert different deformations into recognizable electrical signals based on changes in resistance or capacitance. Recently, conductive hydrogels display promising potential in the fields of wearable devices,[13] implantable biosensors,[14] and artificial skin.[15] Several strategies have been developed to prepare conductive hydrogels, including introduction of ionic salts, direct gelation of conductive materials, combination of hydrogel precursors and conductive fillers, and *in situ* polymerization of conductive polymers within a pre-formed hydrogel.[16–18] Accordingly, conductive hydrogels can be roughly divided into electronically conductive hydrogels (ECHs) and ionically conductive hydrogels (ICHs). As with living organisms, the conduction of electrical signals through the transport of freely charged ions is ubiquitous and extremely important.[19] The electrical conductivity of ICHs exactly depends on the directional movement of free charged ions in the hydrogel network. ICHs are considered as one of ideal candidates for soft matrices in flexible wearable electronic devices because of not only the flexibility similar to biological tissues, but also good electrical properties and high stretchability.[20] However, the extensive applications of ICHs-based flexible sensors are greatly limited under low temperature environments because the sensors become hard, brittle, and non-conductive due to freezing and dehydration of the hydrogels.[21]

Considerable efforts have been devoted to the preparation of frost resistant ICHs for applications at sub-zero temperatures.[21,22] For example, Hu *et al.*[23] reported the preparation of ICHs consisted of hyaluronic acid (HA), chitosan (CS), glycerol, and KCl. The freezing point of the HA/CS/glycerol hydrogel reduced to −37 °C, but the conductivity of the hydrogel was approximate 0.0638 S m^{-1} at room temperature. Liu *et al.*[24] prepared a polyvinyl alcohol (PVA)/Zn^{2+}/ethylene glycol hydrogel, which displayed a conductivity of 0.905 S m^{-1} at −20 °C and 1.503 S m^{-1} at room temperature. Although the introduction of polyols protected the hydrogels against freezing and dehydration under sub-zero temperature,[25] the electrical conductivity of the ICHs was significantly decreased. Inspired by the freezing point decrease of sea water due to the high concentration of various ions, the incorporation of hydratable salts is beneficial to improve both the frost resistance and electrical conductivity of the hydrogels.[26,27] In addition, it is noteworthy that both wearable devices and strain sensors are inevitably in direct contact with the skin in order to ensure the accuracy and stability of the signal, the adhesion of these sensors becomes necessary.[28–30] It is well-known that wearable devices and strain sensors need to be directly adhered on the surface of skin in order to ensure the accuracy and stability of the signal. On the

[a]State Key Laboratory of Advanced Technology for Materials Synthesis and Processing, Biomedical Materials Engineering and Research Center of Hubei Province, Wuhan University of Technology, Wuhan 430070, P. R. China. E-mail: wuqzh@whut.edu.cn
[b]National Engineering Research Center for Nanomedicine, College of Life Science and Technology, Huazhong University of Science and Technology, Wuhan 430074, P. R. China. E-mail: wanjl@hust.edu.cn

other hand, hydrogel-based sensors are usually frozen and become stiff at low temperature, resulting in peeling off from the surface of skin and other interfaces and affecting the signal sensing. Therefore, it is important for the hydrogel-based sensors with adhesion ability at low temperature. Therefore, it is one of great challenges to design and prepare the ICHs with self-adhesion, frost-resistance, and moisture retention for high resolution flexible sensors.

In this study, a novel strategy, naturally inspired by super-adhesive ability of mussel and the decreased freezing point of sea water derived from the increased salinity, has been developed to prepare the ICHs with self-adhesive and frost-resistant ability for high-resolution flexible sensors. As shown in Scheme 1, ICHs were prepared through a facile freeze–thaw cycle combined with salt impregnation method. PVA with excellent flexibility and mechanical property was used as flexible matrix. Inspired by super-adhesive ability of mussel, modification with catechol groups can significantly improve the self-adhesive ability of various polymers. Therefore, catechol molecules were grafted to molecular chains of quaternized chitosan to impart the hydrogels with self-adhesive and electrical conductive ability.[31,32] Meanwhile, catechol groups can form a dynamically reversible metal–ligand bond with Fe^{3+}, which further improves mechanical strengthen of the hydrogel. MXene nanosheets were added to increase not only the movement channel and speed of the ions, but also mechanical strength of the hydrogels.[33–35] The sensors fabricated with the PVA/QCS-C/MXene hydrogel show high sensitivity, significant strain response, and repeatable detection accuracy for monitoring motion of human body, such as bending of finger and elbows, and vocal-cord vibration of throat.

2. Experimental section

2.1 Materials

Poly(vinyl alcohol) (PVA, Degree of alcoholysis: 98–99% (mol mol^{-1})), LiF (99.99%, metals basis), HCl (37%), acetic acid (99.8%) and 3,4-dihydroxybenzaldehyde (DBA, AR, 98%) were bought from Aladdin Biotechnology Co., Ltd., Shanghai, China. MXene (Ti_3AlC_2) powders were purchased from Jilin 11 Technology Co., Ltd., Jilin, China. Sodium borohydride ($NaBH_4$, AR, 99%), chitosan (CS, $M_w = 30\,000$) and glycidyl-trimethylammonium chloride (GTMAC, ≥95%) were purchased

from Macklin Chemistry Co., Ltd., Shanghai, China. All other chemicals (NaCl, KCl, $CaCl_2$, LiCl, $FeCl_3$) were purchased from Sinopharm Chemical Reagent Co., Ltd, Shanghai, China, and utilized without pretreatment. All the water used in the experiment was deionized water, prepared by the ULUP-L-20 ultrapure water mechanism (ULUPURE, Chengdu, China).
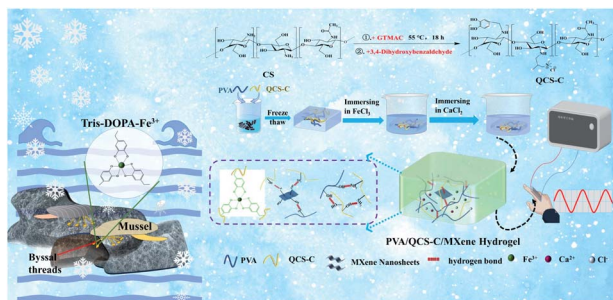
2.2 Experimental section

2.2.1 Synthesis of catechol-modified quaternized chitosan (QCS-C). The QCS was prepared according to a previously reported method with modification. Briefly, 1 g of chitosan was dissolved in 100 mL acetic acid solution (0.5% v/v) with continuous stirring for 12 h. Then the solution was stirred for 18 h at 55 °C after adding 2.82 g of GTMAC. Afterwards, the transparent yellow solution was filtered and the QCS solution was further purified through dialysis (14 000 Da) against DI-water for 3 days. Finally, the purified QCS sponge was obtained by lyophilization with FD-1A-50 lyophilizer (Biocool. Beijing, China).

To modify QCS with catechol, QCS (1 g) sponge was dispersed into aqueous solution (90 mL, pH = 5) under magnetic stirring to form a transparent QCS solution. DBA (4.2895 g) was dissolved in ethanol (25 mL) and added dropwise into the QCS solution. After further stirring at 45 °C for 24 h, $NaBH_4$ (6.5 g) was introduced under vigorous stirring to obtain a turbid suspension. The precipitate was dissolved in water with pH = 3. After dialysis with distilled water for 3 days, QCS-C sponge was obtained by lyophilization.

2.2.2 Preparation of MXene nanosheets. MAXene (Ti_3AlC_2) was etched selectively with a mixture of HCl and LiF to remove the Al layer and prepare MXene nanosheets. In brief, HCl (6 M, 30 mL) was poured into the Teflon beaker (100 mL), and LiF (1.5 g) was added to HCl to produce HF. After that, Ti_3AlC_2 was added slowly to the above solution and the mixture was stirred at 36 °C for 36 h. The obtained product was washed with distilled water and centrifuged at 3500 rpm for 10 min until the pH of the supernatant was higher than 6.0, and the clay-like $Ti_3C_2T_x$ precipitate was obtained. $Ti_3C_2T_x$ clay was then dispersed in distilled water and sonicated for 30 min to peel off the nanosheets. The suspension was centrifuged at 4000 rpm for 10 min to remove unexfoliated MXene nanosheets. MXene nanosheets was subsequently obtained by lyophilization and stored in a 4 °C refrigerator.

2.2.3 Preparation of PVA/QCS-C/MXene hybrid hydrogels. In a typical preparation, MXene aqueous solution at a concentration of 1 mg mL^{-1} was prepared under the ice-bath sonication. QCS-C and PVA (10 wt%) were added into the MXene solution under magnetic stirring at 95 °C for 3 h to form a homogeneous solution. The mixture was poured into the PTFE mold and slowly cooled down at room temperature. Subsequently, the sample was frozen at −20 °C for 19 h, and was unfrozen at room temperature for 5 h. The frozen-unfrozen steps were repeated 3 times. The sample was immersed in $FeCl_3$ aqueous solution (50 mM) for 2 h to obtain the hydrogel, and the residual water on the surface was wiped off. The hydrogel is denoted as PVA/QCS-C$_{xx}$/MXene, and it is

Scheme 1 Schematic illustration of the preparation of PVA/QCS-C/MXene hydrogels for strain sensors.

Paper

abbreviated as P/QC$_{xx}$/M, where "xx" represents the ratio of PVA and QCS-C. For example, "10" in PVA/QCS-C$_{10}$/MXene represents that the content of QCS-C is 10% of PVA. The detailed composition of as-prepared hydrogels was presented in Table 1.

2.2.4 Salt impregnation treatment of the hydrogels. In order to improve the ionic conductivity of the hydrogel, the as-prepared hydrogel was re-immersed in 3M salt solution (Fe^{3+}, Ca^{2+}, Na^+, K^+, Li^+) for 1 h, and the residual water on the surface was wiped off.

2.3 Characterizations

The chemical structure and composition of QCS and QCS-C were characterized through Fourier Transform Infrared spectroscopy (FT-IR, Nexus, Thermo Fisher Scientific-Nicolet IS5, US) in the range of 400 to 4000 cm^{-1} and nuclear magnetic resonance (NMR, AMX-400, Bruker, Switzerland). The crystal structure of MAX and MXene was analyzed through X-ray diffraction (XRD) from 5° to 70° using an X-ray diffractometer (D8 Advance, Bruker, Germany). The morphology and structure of MXene nanosheets and the hydrogels were observed through transmission electron microscope (TEM, JEM-2100 UH, JEOL Japan) and scanning electron microscope (SEM, JSM-7600 F, JEOL, Japan).

2.4 Mechanical tests

The mechanical properties of the hydrogels were determined through a universal material testing machine (AGS-X, SHIMADZU, Japan). The compression strength was tested at a rate of 5 mm min^{-1} using cylindrical hydrogels with a diameter of 15 mm and a height of 10 mm. The compressive elastic modulus was calculated from the slope of the initial linear region of stress–strain curves. The substrate of adhesion experiment is pig skin, glass, rubber, silica gel and PTFE with the size of 40 mm × 15 mm, and the hydrogel is also cut to 15 mm × 15 mm × 2 mm. Triple samples ($n = 3$) were tested for each hydrogel.

2.5 Electromechanical tests of the hydrogels

The electrochemical tests were carried out using the three-electrode system of CHI660E electrochemical workstation (Shanghai Chenhua Co., Ltd., China). The ionic conductivity is calculated as follows:

$$\sigma = \frac{L}{RA}$$

where, L is the thickness of the hydrogels, R is the impedance value, and A is the contact area between the hydrogel and copper electrode.

Electromechanical responses were recorded using the CHI660E electrochemical workstation. The real-time resistance was calculated according to Ohm's law ($R = U/I$), where, U is the applied constant voltage (2 V) and I is the real-time current at different strains monitored by the electrochemical workstation.

The sensing performance at low temperature is carried out in a foam tank containing liquid nitrogen, ice pack and ice.

2.6 Anti-drying experiments of the hydrogels

The hydrogel samples were modelled as cylindrical shapes with a diameter of 15 mm and the high of 10 mm, which were fully exposed at room temperature and the weight changes were recorded according to the time intervals. The weight loss ratio (WLR) was calculated according to the following formula:

$$\text{WLR} = \frac{W_0 - W_S}{W_0} \times 100\%$$

where, WLR is the weight loss ratio, W_0 is the initial mass of the hydrogels, and W_S is the mass of the hydrogels at the selected time point.

3. Results and discussion

The preparation of QCS and QCS-C was analysed through FT-IR and NMR characterizations (Fig. S1 and S2, ESI†), The characteristic peaks at 1392 cm^{-1} and 1470 cm^{-1} in FT-IR spectra can be attributed to the methyl bond of glycidyl-trimethylammonium chloride (GTMAC), indicating that GTMAC was successfully grafted onto the chitosan skeleton.[36] The characteristic peak at 1510 cm^{-1} can be attributed to the C=C aromatic ring vibration, indicating that the catechol groups were successfully grafted to the molecular chain of QCS.[37] In NMR spectra of CS, QCS, and QCS-C, two characteristic peaks appeared at 3.1 ppm and 4.3 ppm, which can be assigned to the trimethylammonium and –NH–CH$_2$– protons of QCS, respectively.[38,39] While the characteristic peak at 6.7–7.0 ppm can be assigned to the catechol group.[40] Therefore, both FT-IR spectra and NMR spectra confirm the successful preparation of QCS-C.

The preparation process of MXene nanosheets was shown in Fig. S3 (ESI†). The phase structure of MXene (Ti$_3$C$_2$) nanosheets was analysed through XRD characterization (Fig. S4a, ESI†). It is obvious that the characteristic peak of Al at 39° disappeared in XRD pattern of MXene, implying that the Al layer was removed by etching. While the shift of the (002) peak to a smaller angle indicates that the interlayer spacing between the MXene nanosheets increased, which is beneficial to the electrical conductivity.[34] TEM image shows that as-prepared MXene nanosheets displayed a typical graphene-like sheet structure with a large specific surface area (Fig. S4b, ESI†). No impurity was observed on the edge and surface of the MXene nanosheets,

Table 1 The detailed composition of the PVA/QCS-C/MXene hydrogels

Hydrogel specimen	QCS-C (mg)	PVA (mg)	MXene (mg mL^{-1})	H$_2$O (g)
PVA/QCS-C$_0$/MXene	0	200	1	1.8
PVA/QCS-C$_5$/MXene	10	190	1	1.8
PVA/QCS-C$_{10}$/MXene	18	182	1	1.8
PVA/QCS-C$_{15}$/MXene	26	174	1	1.8
PVA/QCS-C$_{20}$/MXene	33	167	1	1.8
PVA/QCS-C$_{25}$/MXene	40	160	1	1.8
PVA/QCS-C$_{30}$/MXene	46	154	1	1.8
PVA/QCS-C$_{35}$/MXene	52	148	1	1.8

suggesting without formation of oxides after etching.[41] EDS analysis shows that the surface of MXene nanosheets contains numerous hydrophilic functional groups (–OH, –O, and –F) after etching, which significantly improved dispersion of MXene nanosheets in aqueous environment (Fig. S4c and d, ESI†).[33] An obvious Tyndall effect was observed in MXene aqueous solution under laser pointer irradiation after 12 h of sonication treatment (Fig. S3, ESI†).

The structure of PVA/QCS-C/MXene hydrogels was characterized through SEM observation after freeze-drying (Fig. 1). The typical porous sponge-like structure was observed for the hydrogels with different QCS-C contents (Fig. 1a–f). The porous and interpenetrating structure inside the hydrogels is a major contributor to its ability to absorb and retain large amounts of water, which is also beneficial to the movement of conductive ions. With the increase of the QCS-C content in the hydrogels, the pore size gradually decreased and the structure became denser, which may decrease water swelling and the conductivity of the hydrogels. MXene nanosheets with the lamellar and wrinkled morphology were observed in the porous structure. SEM and EDS images of the PVA/QCS-C$_{15}$/MXene hydrogel (Fig. 1g–i) show that both F and Ti element derived from MXene nanosheets were uniformly dispersed in the hydrogel, demonstrating that MXene nanosheets were uniformly distributed in the hydrogel. This is important to improve conductivity of the hydrogels through providing more movement channels besides water and enhancing the movement speed of the ions.[42,43] The thickness of the hydrogel is 2 mm. As shown in Fig. 1i, the uniform distribution of Cl$^-$ proves that it is easy for salt solution to penetrate hydrogel.
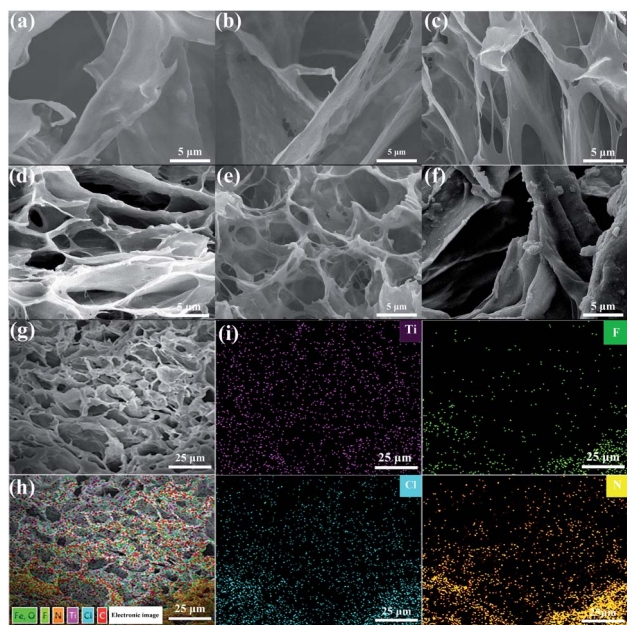
Adhesion strength of the hydrogels on the surface of different substrates (such as glass, rubber, PTFE, pork skin, and silica gel) were measured (Fig. S5 and S6, ESI†). Fig. S5† shows schematic diagram of adhesion experiment. Fig. S6† shows that the lap shear strength was approximately 30.33 ± 3.20 kPa, 10.125 ± 1.75 kPa, 13.18 ± 1.71 kPa, 19.92 ± 1.44 kPa, and 10.23 ± 3.11 kPa for pork skin, glass, rubber, PTFE, and silica gel, respectively. A qualitative analysis on adhesion strength of the hydrogel at low temperature was carried out in a low temperature box (Fig. S7†). Results show that these materials tightly sticked at low temperatures.

The influence of the QCS-C content on mechanical strength of as-prepared PVA/QCS-C/MXene hydrogels was studied through measuring compressive modulus of the hydrogels before and after cross-linking by Fe^{3+} ions (Fig. 2a). Results show that the compressive modulus of the hydrogels decreased with the increase of the QCS-C content, which was obviously improved after the cross-linking treatment with Fe^{3+} ions. The compressive modulus of the PVA/QCS-C/MXene hydrogels with the QCS-C content of 15% was increased from 83.7 kPa to 97.4 kPa after cross-linking treatment. It is speculated that the addition of QCS-C affects the network structure of PVA and therefore decreases the mechanical strength of the hydrogels, while the coordination interaction between Fe^{3+} ions and catechol groups of QCS-C is beneficial to partial offset the
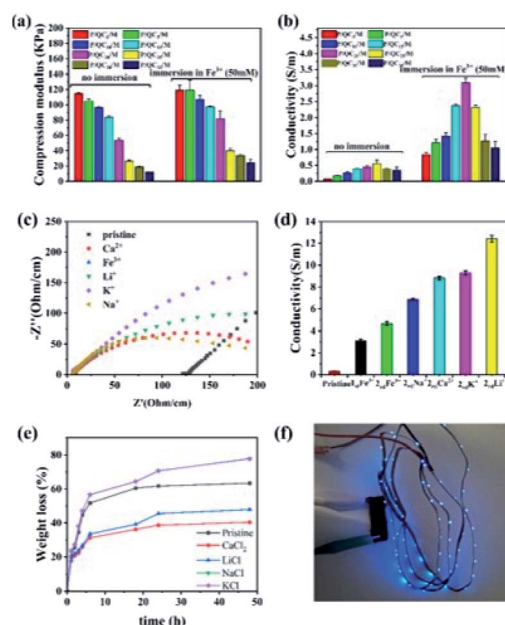

Fig. 1 SEM images of PVA/QCS-C/MXene hydrogels with different QCS-C contents. (a) PVA/QSC-C$_5$/MXene, (b) PVA/QCS-C$_{10}$/MXene, (c) PVA/QCS-C$_{15}$/MXene, (d) PVA/QCS-C$_{20}$/MXene, (e) PVA/QCS-C$_{25}$/MXene, (f) PVA/QCS-C$_{30}$/MXene, (g) SEM image of PVA/QCS-C$_{15}$/MXene after FeCl$_3$ cross-linking, (h) and (i) EDS images of (g).

Fig. 2 (a) Effect of the QCS-C content and Fe^{3+} cross-linking treatment on compressive modulus of the PVA/QCS-C/MXene hydrogels. (b) Effect of the QCS-C content and Fe^{3+} cross-linking treatment on the conductivity of the PVA/QCS-C/MXene hydrogels. (c) EIS-Nyquist diagram of ionic conductivity of the PVA/QCS-C$_{15}$/MXene hydrogel after impregnated in different salt solutions. (d) Ionic conductivity of the PVA/QCS-C$_{15}$/MXene hydrogel after different salt impregnation treatments. (e) Water retention capacity of the PVA/QCS-C$_{15}$/MXene hydrogel after different salt impregnation treatment. (f) The LED strip was lit up using the PVA/QCS-C$_{15}$/MXene hydrogel as the conductor after Fe^{3+} cross-linking and CaCl$_2$ impregnation treatment.

mechanical strength due to the formation of double-network-like structure inside the hydrogels.[34,44]

The conductivity of the PVA/QCS-C/MXene hydrogels with different QCS-C contents was affected by cross-linking treatment with Fe^{3+}. The highest conductivity of the hydrogels was approximate 0.4 S m^{-1} before Fe^{3+} cross-linking, which was increased to approximate 3.1 S m^{-1} after cross-linking treatment (Fig. 2b). It is noteworthy that the conductivity of the hydrogels after cross-linking treatment was positively proportional to the QCS-C content, which was sharply decreased at the higher QCS-C content of 30%. It is possible that the higher content of positively charged QCS-C could attract the negatively charged MXene nanosheets, and result in agglomeration and compact structure, which is not conducive to ion movement.[45] In addition, the higher content of positively charged QCS-C attracts more anions, which also decreases the conductivity of the hydrogels.

In order to further improve the conductivity and impart the higher ability of frost-resistance and water retention to the hydrogels, a salt impregnation treatment was carried out using different salt solutions (NaCl, KCl, LiCl, $CaCl_2$ and $FeCl_3$) after Fe^{3+} cross-linking treatment. The resistance of the hydrogels was measured through electrochemical impedance spectroscopy (EIS). The X intercept of EIS curves represents the impedance of the hydrogels (Fig. 2c). Results show that salt impregnation treatment significantly decreased the impedance of the hydrogels. Compared with the PVA/QCS-C_{15}/MXene hydrogel without and with Fe^{3+} cross-linking treatment, the hydrogels displayed significantly higher conductivity after salt impregnation treatment. The electrical conductivity was increased from approximate 0.31 ± 0.01 and 3.10 ± 0.15 S m^{-1} to 12.42 ± 0.31, 9.29 ± 0.20, 8.82 ± 0.16, 6.87 ± 0.10, and 4.68 ± 0.17 S m^{-1}, corresponding to salt impregnation treatment with LiCl, KCl, $CaCl_2$, NaCl, and $FeCl_3$, respectively. Water retention capacity was evaluated through measuring the weight loss of the hydrogels under room temperature and 40%RH conditions (Fig. 2e). The PVA/QCS-C_{15}/MXene hydrogel without Fe^{3+} cross-linking treatment lost 63.4% of its moisture and became rigid. The hydrogels after cross-linking and salt impregnation treatment with NaCl and KCl lost 77.9% and 77.7% of their moisture, respectively. It is interesting that salt impregnation treatment with LiCl and $CaCl_2$ effectively suppressed the evaporation of water, and the weight loss was reduced to 47.9% and 40.4%, respectively. These results show that the PVA/QCS-C_{15}/MXene hydrogel after Fe^{3+} cross-linking and $CaCl_2$ impregnation treatment displayed both the high conductivity and water retention capacity. The LED strip was lit up using the PVA/QCS-C_{15}/MXene hydrogel as the conductor (Fig. 2f).

Fig. 3 and 4 shows the evaluations on the frost-resistant and self-adhesive ability of the PVA/QCS-C_{15}/M hydrogel after Fe^{3+} cross-linking and $CaCl_2$ impregnation treatment. After placed at −20 °C for 24 h, the hydrogel without $CaCl_2$ impregnation treatment became brittle and broken off when bent, while the hydrogel with $CaCl_2$ impregnation treatment was still flexible without fracture. The condensation temperature of the hydrogels measured through DSC technique decreased from approximate −9.7 °C to −44.7 °C after $CaCl_2$ impregnation
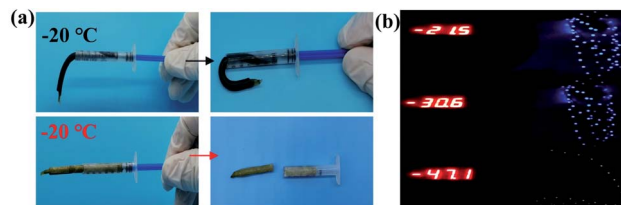

Fig. 3 Frost-resistance and self-adhesion of the PVA/QCS-C_{15}/MXene hydrogel after Fe^{3+} cross-linking and $CaCl_2$ impregnation treatment. (a) Frost-resistance of the hydrogel without and with $CaCl_2$ impregnation treatment after being placed at −20 °C for 24 h. (b) Conductivity of the hydrogel with $CaCl_2$ impregnation treatment placed in cryogenic tank. The LED strip was lit up and remained bright until −47.1 °C.

treatment. The frost-resistance of the hydrogel was further evaluated by placing the hydrogel in a cryogenic tank containing liquid nitrogen. Fig. 3b shows that the LED strip remains bright at a temperature of approximate −47.1 °C, indicating that the PVA/QCS-C/MXene hydrogel has good frost-resistance. It is speculated that the crystallization of water in the hydrogel was suppressed due to the introduction of $CaCl_2$,[7,46] which resulted in a sharp decrease in the freezing point of the PVA/QCS-C_{15}/M hydrogel.

The self-adhesive ability of the hydrogel was evaluated using different substrates. As shown in Fig. 4a, the hydrogel was ready to easily adhere to the surface of different substrates, including polytetrafluoroethylene, glass, rubber, and silica gel. In addition, the hydrogel can be remodelled into different geometric shapes, such as rectangles, horses, puzzles, and cherry blossoms, after dissolved into aqueous solution at 95 °C (Fig. 4b). We also measured the tensile and compressive properties of the hydrogel at low temperature. As shown in Fig. S8† (ESI), the compressive strength and tensile strength of the hydrogel at −30 °C was approximately 3.45 ± 0.45 MPa and 135.25 ± 11.53 kPa, respectively.

ICH-based sensors display promising potential to monitor a wide range of human body motion, including the bending of knee, elbow joint, and finger at different angles, as well as vocal cord vibration of throat. The sensing performance of the PVA/QCS-C_{15}/MXene hydrogel after Fe^{3+} cross-linking and $CaCl_2$ impregnation treatment was studied. Fig. 5a–c show that the hydrogel sensor can instantly detect the different signals
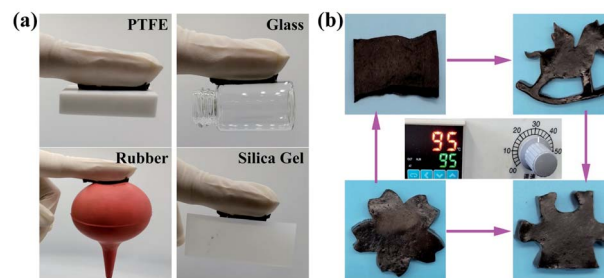

Fig. 4 (a) Digital photos of the hydrogel adhered to the surface of different substrates. (b) Re-modelling the hydrogel into different morphologies after dissolved into aqueous solution at 95 °C.
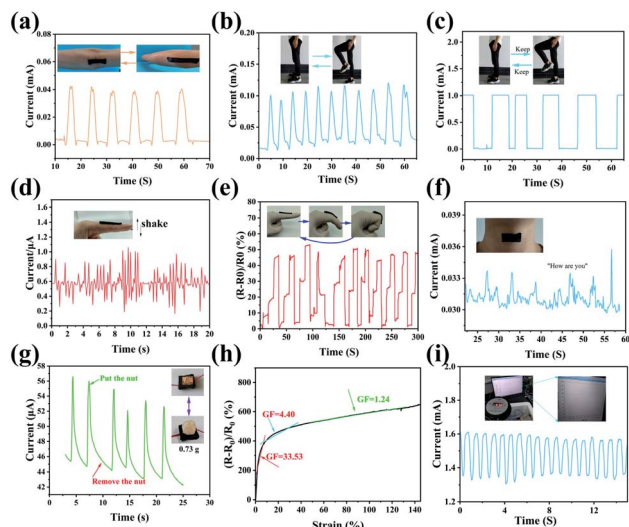
Fig. 5 Evaluations on sensing performance of the PVA/QCS-C$_{15}$/MXene hydrogel sensor under different situations. (a) Motion of elbow, (b) and (c) motion of knee, (d) and (e) motion of finger, (f) "Taking and placing" a nut with a mass of 0.73 g, (g) vocal-cord vibration of throat, (h) relative resistance-tensile strain curve of the hydrogel sensors, (i) motion of finger at low temperature (-47.0 °C).

derived from body movements (elbow and knee bending). The high resolution of the hydrogel sensor was further evaluated through monitoring the deformation induced by bending, vibration, and pressure. Two motion modes of the finger were tested (Fig. 5d and e), *i.e.*, waving up and down and bending at different angles (0°, 45° and 90°). The vocal-cord vibration of throat was tested when speaking "how are you" (Fig. 5f), and pressure change was tested through "taking and placing" a Macadamia nut with a mass of 0.73 g (Fig. 5g). Results show that the hydrogel sensor can precisely detect the small deformation induced the bending of the finger, vocal-cord vibration of throat, and pressure change of small weight. Fig. 5h shows the relative resistance-tensile strain curve of the hydrogel sensor with a gauge factor of approximate 33.53 at low strain (0–10%). Fig. 5i shows that the hydrogel sensor can precisely respond to the bending of the finger at -47.0 °C. These results demonstrate good frost-resistance and ionically conductivity of the PVA/QCS-C$_{15}$/M hydrogel as sensors. The response time is 0.18 s at room temperature and 0.2 s at low temperature (-40 °C) (Fig. S9, ESI†). This is because ions move faster at room temperature than at low temperature, and small deformation can cause faster response. The sensor signal is still stable after 100 cycles as shown in Fig. S10 (ESI†).

4. Conclusions

In summary, nature-inspired strategy has been developed to prepare the PVA/QCS-C/MXene hydrogels with the high conductivity, self-adhesion, frost-resistance, and water retention capacity. These results provide not only a novel nature-inspired strategy for the preparation of functional ICHs, but

also a promising ICH for applications as high-performance sensors and wearable electronic devices.

Conflicts of interest

There are no conflicts to declare.

Acknowledgements

Notes and references

1 S. Li, X. Zhou, Y. Dong and J. Li, *Macromol. Rapid Commun.*, 2020, **41**(23), 2000444.
2 R. Liu, L. He, M. Cao, Z. Sun, R. Zhu and Y. Li, *Front. Chem.*, 2021, **9**, 539678.
3 S. Masuki, M. Morikawa and H. Nose, *Compr. Physiol.*, 2020, **10**, 1207–1240.
4 K. R. Singh, V. Nayak, J. Singh and R. P. Singh, *Mater. Lett.*, 2021, **304**, 130614.
5 D. Li, D. Yao, X. Gao, C. Lu, M. Zhang and H. Fang, *J. Mater. Sci.: Mater. Med.*, 2021, **32**, 27305–27317.
6 S. J. Wang, J. H. Lin, Z. Xu and Z. P. Xu, *Composites, Part A*, 2021, **143**, 106318.
7 G. K. K. Chik, N. Xiao, X. Ji, A. C. O. Tsang, G. K. K. Leung, S. Zhang, C. Tin and P. K. L. Chan, *Adv. Mater. Technol.*, 2022, **7**, 2200143.
8 H. Dong, J. C. Sun, X. M. Liu, X. D. Jiang and S. W. Lu, *ACS Appl. Mater. Interfaces*, 2022, **14**, 15504–15516.
9 J. Bang, Y. Jung, H. Kim, D. Kim, M. Cho and S. H. Ko, *Nano-Micro Lett.*, 2022, **14**(1), 49.
10 D. Jiang, Z. Liu, Z. Xiao, Z. Qian, Y. Sun, Z. Zeng and R. Wang, *J. Mater. Chem. A*, 2021, **10**, 89–121.
11 C. Han, X. Li, Y. Liu, Y. Tang, M. Liu, X. Li, C. Shao, J. Ma and Y. Liu, *Adv. Sci.*, 2021, **8**(23), 2102471.
12 D. Li, J. Du, Y. Tang, K. Liang, Y. Wang, H. Ren, R. Wang, L. Meng, B. Zhu and Y. Li, *Adv. Funct. Mater.*, 2021, **31**(47), 2105887.
13 Y. Huang, M. Zhong, F. K. Shi, X. Y. Liu, Z. J. Tang, Y. K. Wang, Y. Huang, H. Q. Hou, X. M. Xie and C. Y. Zhi, *Angew. Chem., Int. Ed.*, 2017, **56**, 9141–9145.
14 Z. Liu, Y. Wang, Y. Ren, G. Jin, C. Zhang, W. Chen and F. Yan, *Mater. Horiz.*, 2020, **7**, 919–927.
15 Y. Wu, S. Sun, A. Geng, L. Wang, C. Song, L. Xu, C. Jia, J. Shi and L. Gan, *Compos. Sci. Technol.*, 2020, **196**, 108226.
16 Z. Chen, Y. Chen, M. S. Hedenqvist, C. Chen, C. Cai, H. Li, H. Liu and J. Fu, *J. Mater. Chem. B*, 2021, **9**, 2561–2583.
17 Q. Peng, J. Chen, T. Wang, X. Peng, J. Liu, X. Wang, J. Wang and H. Zeng, *Infomat*, 2020, **2**, 843–865.
18 J. Xu, Y.-L. Tsai and S.-h. Hsu, *Molecules*, 2020, **25**(22), 5296.
19 C. Keplinger, J. Y. Sun, C. C. Foo, P. Rothemund, G. M. Whitesides and Z. G. Suo, *Science*, 2013, **341**, 984–987.
20 S. Hong, Y. Yuan, C. Z. Liu, W. M. Chen, L. Chen, H. L. Lian and H. Liimatainen, *J. Mater. Chem. C*, 2020, **8**, 550–560.

21 Y. Jian, S. Handschuh-Wang, J. Zhang, W. Lu, X. Zhou and T. Chen, *Mater. Horiz.*, 2021, **8**, 351–369.

22 S. Li, H. Pan, Y. Wang and J. Sun, *J. Mater. Chem. A*, 2020, **8**, 3667–3675.

23 Y. Hu, N. Liu, K. Chen, M. Liu, F. Wang, P. Liu, Y. Zhang, T. Zhang and X. Xiao, *Front. Bioeng. Biotechnol.*, 2022, **10**, 837750.

24 J. Liu, Z. Khanam, S. Ahmed, T. Wang, H. Wang and S. Song, *ACS Appl. Mater. Interfaces*, 2021, **13**, 16454–16468.

25 J. Wu, Z. Wu, W. Huang, X. Yang, Y. Liang, K. Tao, B.-R. Yang, W. Shi and X. Xie, *ACS Appl. Mater. Interfaces*, 2020, **12**, 52070–52081.

26 Z. Wu, W. Shi, H. Ding, B. Zhong, W. Huang, Y. Zhou, X. Gui, X. Xie and J. Wu, *J. Mater. Chem. C*, 2021, **9**, 13668–13679.

27 S. Liu, R. Zheng, S. Chen, Y. Wu, H. Liu, P. Wang, Z. Deng and L. Liu, *J. Mater. Chem. C*, 2018, **6**, 4183–4190.

28 X. Wang, B. Yang, J. Liu and C. Yang, *J. Mater. Chem. A*, 2017, **5**, 1176–1183.

29 W. Sun, J. Yang, X. Ji, H. Jiang, L. Gai, X. Li and L. Liu, *Sustainable Mater. Technol.*, 2022, **32**, e00437.

30 C. Lu, J. Qiu, W. Zhao, E. Sakai, G. Zhang, R. Nobe, M. Kudo and T. Komiyama, *Int. J. Biol. Macromol.*, 2021, **188**, 534–541.

31 K. Torpol, S. Sriwattana, J. Sangsuwan, P. Wiriyacharee and W. Prinyawiwatkul, *Int. J. Food Sci. Technol.*, 2019, **54**, 2064–2074.

32 T. Yang, M. Wang, F. Jia, X. Ren and G. Gao, *J. Mater. Chem. C*, 2020, **8**, 2326–2335.

33 T. Zhou, C. Wu, Y. Wang, A. P. Tomsia, M. Li, E. Saiz, S. Fang, R. H. Baughman, L. Jiang and Q. Cheng, *Nat. Commun.*, 2020, **11**(1), 2077.

34 Y. Feng, H. Liu, W. Zhu, L. Guan, X. Yang, A. V. Zvyagin, Y. Zhao, C. Shen, B. Yang and Q. Lin, *Adv. Funct. Mater.*, 2021, **31**(47), 2105887.

35 S.-N. Li, Z.-R. Yu, B.-F. Guo, K.-Y. Guo, Y. Li, L.-X. Gong, L. Zhao, J. Bae and L.-C. Tang, *Nano Energy*, 2021, **90**, 106502.

36 M. R. Kasaal, *Carbohydr. Polym.*, 2008, **71**, 497–508.

37 E. Jeevithan, W. Wu, N. Wang, H. Lan and B. Bao, *Process Biochem.*, 2014, **49**, 1767–1777.

38 X. Li, R. Xing, C. Xu, S. Liu, Y. Qin, K. Li, H. Yu and P. Li, *Carbohydr. Polym.*, 2021, **264**, 118050.

39 A. Zeng, Y. Wang, D. Li, J. Guo and Q. Chen, *Chin. J. Chem. Eng.*, 2021, **32**, 462–471.

40 Z. Zheng, S. Bian, Z. Li, Z. Zhang, Y. Liu, X. Zhai, H. Pan and X. Zhao, *Carbohydr. Polym.*, 2020, **249**, 116826.

41 T. Yu, X. Lei, H. Chen, K. Fan, D. Wang and Y. Gao, *Ceram. Int.*, 2022, **48**, 1382–1393.

42 S. Li, Z. Fan, G. Wu, Y. Shao, Z. Xia, C. Wei, F. Shen, X. Tong, J. Yu, K. Chen, M. Wang, Y. Zhao, Z. Luo, M. Jian, J. Sun, R. B. Kaner and Y. Shao, *ACS Nano*, 2021, **15**, 7821–7832.

43 Y. Shi, B. Li, Q. Zhu, K. Shen, W. Tang, Q. Xiang, W. Chen, C. Liu, J. Luo and S. Yang, *Adv. Energy Mater.*, 2020, **10**(9), 1903534.

44 F. Song, J. Zhang, J. Lu, Y. Cheng, Y. Tao, C. Shao and H. Wang, *Int. J. Biol. Macromol.*, 2021, **189**, 183–193.

45 V. Kamysbayev, A. S. Filatov, H. Hu, X. Rui, F. Lagunas, D. Wang, R. F. Klie and D. V. Talapin, *Science*, 2020, **369**, 979–983.

46 K. Nilssen, A. Klein-Paste and J. Wahlin, *Transp. Res. Rec.*, 2018, **2672**, 158–166.